Magnetohydrodynamics, natural convection and entropy generation of CuO-water nanofluid in an I-shape enclosure - A numerical study

Ali Malekpour[1], Nader Karimi[2,3*], Amirfarhang Mehdizadeh[3]
[1]Shahrekord University, Faculty of Engineering, P.O. Box 115, Shahrekord, Iran
[2]School of Engineering, University of Glasgow, Glasgow G12 8QQ, United Kingdom
[3] School of Computing and Engineering, Civil and Mechanical Engineering Department, University of Missouri-Kansas City, Kansas City, MO, 64110, USA

Abstract This paper presents a numerical study of the magnetohydrodynamics, natural convection and thermodynamic irreversibilities in an I-shape enclosure, filled with CuO-water nanofluid and subject to a uniform magnetic field. The lateral walls of the enclosure are maintained at different but constant temperatures, while the top and bottom surfaces are adiabatic. The Brownian motion of the nanoparticles is taken into account and an extensive parametric study is conducted. This involves variation of Rayleigh and Hartmann numbers, and the concentration of nanoparticles and also the geometrical specifications of the enclosure. Further, the behaviours of streamlines and isotherms under varying parameters are visualised. Unlike that in other configurations, the rate of heat transfer in the I-shaped enclosure appears to be highly location dependent and convection from particular surfaces dominates the heat transfer process. It is shown that interactions between the magnetic field and natural convection currents in the investigated enclosure can lead to some peculiarities in the thermal behaviour of the system. The results also demonstrate that different parts of the enclosure may feature significantly different levels of heat transfer sensitivity to the applied magnetic field. Further, analysis of entropy generation indicates that the irreversibility of the system is a strong function of the geometrical parameters and that the variations in these parameters can minimise the total generation of entropy. This study clearly shows that ignoring the exact shape of the enclosure may result in major errors in the prediction of heat transfer and second law performances of the system.

Keywords: Nanofluid; Entropy generation; Natural convection; Magnetohydrodynamics; I-shape enclosure

Nomenclature

a	geometric parameter, m
A	dimensionless geometric parameter, a/L
B_0	magnetic field strength
b	geometric parameter, m
B	dimensionless geometric parameter, b/L
C_p	specific heat, $J.kg^{-1}.K^{-1}$
g	gravitational acceleration, $m.s^{-2}$
Ha	Hartmann number, $B_0 L\left(\sigma_{nf}/\rho_{nf}\nu_f\right)^{0.5}$
T	temperature, K
u,v	velocity components in x,y directions, $m.s^{-1}$
U,V	dimensionless velocity components $(uL/\alpha_f, vL/\alpha_f)$
W	heat source length, m
W	dimensionless heat source length (w/L)
x,y	Cartesian coordinates, m
X,Y	dimensionless coordinates $(x/L, y/L)$

Greek symbols

α	thermal diffusivity, $m^2.s^{-1}$

k	thermal conductivity, $W.m^{-1}K^{-1}$	β	thermal expansion coefficient, K^{-1}
L	length and height of enclosure, m	ϕ	volumetric concentration of nanoparticles
Nu	local Nusselt number on the heat source	μ	dynamic viscosity, $N.s.m^{-2}$
Nu_m	average Nusselt number	ν	kinematic viscosity, $m^2.s^{-1}$
Nu_m^*	Nusselt ratio, $Nu_m/Nu_{m,\ Ha=0}$	θ	dimensionless temperature $(T-T_c)/(T_h-T_c)$
Nu_m^{**}	Nusselt ratio, $Nu_m/Nu_{m,\ \varphi=0}$	ρ	density, $kg.m^{-3}$
		λ	irreversibility distribution ratio
p	fluid pressure, Pa	ψ	stream function
$\bar{p}$	modified pressure ($p+\rho_c g y$)	**Subscripts**	
P	dimensionless pressure ($\bar{p}L^2/\rho_{nf}\alpha_f^2$)	c	cold wall
Pr	Prandtl number (ν_f/α_f)	eff	effective
R_s	radius of nanoparticles, nm	eq	equivalent
Ra	Rayleigh number, ($g\beta_f L^3(T_h-T_c)/\nu_f\ \alpha_f$)	f	fluid (pure)
S_{gen}	Entropy Generation	h	heat source
		nf	nanofluid
		S	nanoparticle

1. Introduction

The last two decades have witnessed an exceptionally rapid growth in the research activities on nanofluids [1,2]. Suspension of nanoparticles in a liquid increases the thermal conductivity of the fluid [3,4]. The augmented conductivity of the base fluid then results in improvements in heat convection in either of forced [5,6,7] or natural [8] modes. The general area of convective heat transfer in nanofluids has received significant attention [2,3,9]. In particular, natural convection of nanofluids has been vastly studied [3,8]. This is, perhaps, reflective of the growing significance of natural convection in modern applications such as electronics cooling [10]. It is also representative of the fact that there exists a considerable potential for improving natural convection through using nanofluids [9].

Many scholars have contributed to the field of natural convection of nanofluids and an exhaustive review of literature in this area is beyond the current discourse. Amongst other researchers, Ghasemi and Aminossadati [11], Khanfar et al. [12], Kefayati et al. [13] and Lai and Yang [14] conducted detailed studies on this problem. These authors have all reported an enhancement of convective heat transfer through increasing the volumetric concentration of nanoparticles in the base fluid. Mahmoudi et al. [15] numerically investigated the natural convection of water-copper nanofluid in a square enclosure containing a horizontal heat source on the vertical side of the enclosure. They concluded that the dimensions of the heat source are the most influential parameter dominating the flow and heat transfer properties. Their results also showed that for a specified length of heat

source and Rayleigh number, the average Nusselt number increases linearly with the increase in nanoparticles volume fraction [15].

Heat transfer in the presence of magnetic effects is an important necessity in a number of engineering applications including electric propulsion for space exploration, crystal growth in liquids, electronic packages and microelectronic devices. In almost all these applications natural convection is of primary importance. Magnetic field generates Lorentz force in electrically conducting fluids. This acts as a body force, which can then interact with buoyancy forces in the fluid and hence affect the natural convection of heat in the system [16]. Hamed et al. [17] and Gavili et al. [18] experimentally measured the effects of magnetic fields on heat transfer from vertical surfaces. They showed that intensifying the magnetic field reduces the velocity of the fluid flow. In keeping with this finding, other researchers showed that the modification of heat transfer rate by magnetic effects could be rather significant [19-21].

Over many years of research on natural convection of ordinary fluids, a large number of configurations have been investigated [22]. It is now well-documented that natural convection in enclosures is heavily dependent upon the geometry and configuration of the enclosure [23-25]. In recent years, some of these configurations have been re-investigated through considering natural convection of nanofluids [26]. Yet, the diversity of applications and the complexity of nanofluid convection under magnetic effects warrants further extension of these studies to the less explored configurations. Early works on simple rectangular enclosures filled by ordinary fluids and subject to magnetic fields were conducted by Sanokawa [27] and Ozoe and Okada [28]. Later Rudaiah et al. [29] numerically investigated natural convection in an ordinary fluid in the presence of a magnetic field and within a simple cubic enclosure. These authors showed that the magnetic field could significantly suppress the motion of the fluid inside the enclosure and therefore reduce the rate of heat transfer [29]. Similar conclusions were made by Pirmohammadi et al. [30] for tilted enclosures and Chamkha et al. [31] in an enclosure with internal heat generation. These studies clearly demonstrated that the application of magnetic fields to enclosures impedes the transfer of heat by natural convection. Despite this general qualitative trend, quantitate aspects of the problem were found strongly dependent upon the configuration and geometry of the enclosure [29-32].

Improved thermal conductivity of nanofluid is expected to constructively affect the heat transfer process and boost the thermal performance of the system. This notion has been investigated in a series of numerical studies by Sheikholeslami and Ganji and their co-workers, e. g. [33-35]. Further, a wide variety of configurations have been analysed by other authors [21,36,37]. In particular, configuration with curved walls [38] and those containing multiphase-phase fluids [38, 39] have been extensively analysed. Additional physical effects such as non-Newtonian and the slip velocities have been also considered [40,41]. These studies showed that similar to that encountered in ordinary fluids, the enclosures filled with nanofluid lose their heat transfer capability should the magnetic field be intensified. Nonetheless, the use of nanofluid leads to a higher average Nusselt number compared to those calculated for the ordinary fluids in the same configurations [33, 34,37].

In thermo-fluidic systems, energy quality losses inevitably occur as a result of irreversibilities. Generally, the extent of these irreversibilities can be quantified by entropy generation rate. The aim of entropy generation analysis is to understand how to minimise entropy generation, thereby maximising the energy available to do useful work [42–44]. In recent years, entropy generation analysis have been extended to MHD natural convection of nanofluid in enclosures. Hajialigal et al. [45] have discussed the influences of magnetic field on

mixed convection and entropy generation in nanofluid within three-dimensional microchannels. It was highlighted that as the strength of the magnetic field and the volume fraction of nanoparticles increase, the total entropy generation decreases. Mehrez et al. [46] have investigated the impacts of MHD on transfer of heat and entropy generation in a cavity filled with nanofluid. It was found that increasing the volume fraction of nanoparticles results in an enhancement of the average Nusselt number and also intensifies entropy generation. In another recent study Kefayati and Sidik [47] studied entropy generation within a non-Newtonian nanofluid inside an inclined cavity. The results showed enhancement in fluid friction and heat transfer irreversibility with increasing Rayleigh number. Fersadou et al. [48] conducted a numerical study to analyse the effect of magnetic field on entropy generation inside a vertical porous channel filled with Cu-water nanofluid. They also showed that nanoparticle addition increases the entropy generation of the system.

An important fact deducted from the literature is the existence of a strong configurational dependency in the problems involving natural convection in enclosures. Consideration of magnetic fields and nanofluids further intensifies this dependency. Importantly, the primary application of magnetohydrodynamic cooling is in electronic devices, in which the enclosures might be manufactured in a wide range of shapes [10]. In a recent review, Sheikholeslami and Ganji have provided a list of nanofluid enclosures, which have been theoretically and numerically investigated [26]. These include different enclosures with flat walls [49], spherical and cylindrical shapes [50], cylindrical configurations [51], titled enclosures [52] and a wealth of configurations with curved walls, e.g. [38]. It follows from this list that although a large number of configurations have been analysed, some classes of enclosures remain almost entirely unexplored. For instance, combined enclosures consisting of a number of interconnected simpler enclosures have received very little attention. This is surprising as in practice implementation of more complex enclosures is much more likely than those of simple geometry. Thus, analysis of more complex configurations is clearly the next step in the study of natural convection of nanofluids under magnetic effects.

Towards this aim, the current work considers an I-shape enclosure filled with water-CuO nanofluid and under the influence of a horizontally-applied magnetic field. To the best the authors' knowledge, currently there is no study in the open literature on this particular problem. The I-shape enclosure may represent the cooling of electronic components with a non-planar wall. This can include a multi-pieces electronic chip or an electronic micro-coil influenced by the magnetic field. The study involves investigation of coupled hydrodynamic and thermal problems for varying values of Hartman and Rayleigh numbers and the volumetric concentration of nanoparticles. Also of interest are the influences of aspect ratio of the investigated enclosure upon the qualitative and quantitative behaviours of the thermal system.

2. Problem configuration and numerical methods

Figure 1 shows a schematic view of the problem under investigation. This includes an I-shape enclosure with the left walls maintained at high temperature, T_h, and the right walls exposed to a low temperature, T_c. The bottom and top surfaces of the enclosure are assumed to be thermally insulated. The enclosure is filled with water-CuO nanofluid and is also subject to a constant magnetic field B_0 along the x-axis.

2.1. Assumptions and governing equations

The following assumptions are made throughout the current study.

- The nanoparticles and water are in local thermal equilibrium and the nanofluid is a Newtonian and incompressible fluid.
- The flow is considered to be laminar, steady and two-dimensional and radiative heat transfer is ignored.
- The displacement current, induced magnetic field, dissipation and Joule heating are neglected and there is a no-slip boundary condition on all enclosure walls.

The governing equations of continuity, momentum and transport of thermal energy can be, respectively, written in non-dimensional forms as follows [34].

The equation of continuity reduces to

$$\frac{\partial U}{\partial X}+\frac{\partial V}{\partial Y}=0. \tag{1}$$

Momentum equation in X direction is written as

$$U\frac{\partial U}{\partial X}+V\frac{\partial U}{\partial Y}=-\frac{\partial P}{\partial X}+\frac{\mu_{nf}}{\rho_{nf}\alpha_f}\left(\frac{\partial^2 U}{\partial^2 X}+\frac{\partial^2 U}{\partial^2 Y}\right), \tag{2}$$

and that for Y direction becomes

$$U\frac{\partial V}{\partial X}+V\frac{\partial V}{\partial Y}=-\frac{\partial P}{\partial Y}+\frac{\mu_{nf}}{\rho_{nf}\alpha_f}\left(\frac{\partial^2 V}{\partial^2 X}+\frac{\partial^2 V}{\partial^2 Y}\right)-\mathrm{Ha}^2.\mathrm{Pr}V+\mathrm{Ra}.\mathrm{Pr}\frac{(\rho\beta)_{nf}}{\rho_{nf}\beta_f}\theta. \tag{3}$$

Further, the transport of thermal energy takes the form of

$$U\frac{\partial \theta}{\partial X}+V\frac{\partial \theta}{\partial Y}=\frac{\alpha_{nf}}{\alpha_f}\left(\frac{\partial^2 \theta}{\partial X^2}+\frac{\partial^2 \theta}{\partial Y^2}\right), \tag{4}$$

where the following non-dimensional parameters are used in the analysis.

$$X=\frac{x}{L},\quad Y=\frac{y}{L},\quad A=\frac{a}{L},\quad B=\frac{b}{L}$$
$$U=\frac{u\,L}{\alpha_f},\quad V=\frac{v\,L}{\alpha_f},\quad P=\frac{\overline{p}\,L^2}{\rho_{nf}\alpha_f^2},\quad \theta=\frac{T-T_c}{T_h-T_c} \tag{5}$$

In these equations, L is the length of the enclosure and other variables have been defined in the nomenclature. The non-dimensional groups including Rayleigh, Prandtl and Hartmann numbers are defined as follows,

$$\mathrm{Ra}=\frac{g\beta_f L^3(T_h-T_c)}{\nu_f\alpha_f},\qquad \mathrm{Ha}=B_0L\sqrt{\frac{\sigma_{nf}}{\rho_{nf}\nu_f}},\qquad \mathrm{Pr}=\frac{\nu_f}{\alpha_f}. \tag{6}$$

Further, the non-dimensional boundary conditions can be summarised as,

- along all the walls of the enclosure $U = V = 0$
- along the horizontal walls of the enclosure $\partial\theta / \partial Y = 0$ (7)
- along the left walls of the enclosure $\theta = 1$
- along the right walls of the enclosure $\theta = 0$

The rate of heat transfer can be expressed in terms of Nusselt number. The local Nusselt number on the hot walls is defined as

$$\mathrm{Nu}(S) = -\frac{k_{nf}}{k_f}\left(\frac{\partial\theta}{\partial N}\right)_{wall}, \tag{8}$$

in which, N can be either of the dimensionless coordinates of X or Y.

The average Nusselt number is obtained by integrating the local Nusselt number over the hot walls. That is

$$\mathrm{Nu}_m = \frac{1}{S}\int_0^S \mathrm{Nu}(S)dS \quad , \tag{9}$$

where S is the surface area of the hot walls.

The local entropy generation equation given by Bejan [42] can be adopted for nanofluid as [53]:

$$s_{gen} = \frac{k_{nf}}{T_o^2}\left[\left(\frac{\partial T}{\partial x}\right)^2 + \left(\frac{\partial T}{\partial y}\right)^2\right] + \frac{\mu_{nf}}{T_o}\left\{2\left[\left(\frac{\partial u}{\partial x}\right)^2 + \left(\frac{\partial v}{\partial y}\right)^2\right] + \left(\frac{\partial u}{\partial y} + \frac{\partial v}{\partial x}\right)^2\right\} \tag{10}$$

where $T_0 = (T_H + T_C)/2$. By using dimensionless parameters, the dimensionless local entropy generation reduces to

$$S_{gen} = \frac{k_{nf}}{k_f}\left[\left(\frac{\partial\theta}{\partial X}\right)^2 + \left(\frac{\partial\theta}{\partial Y}\right)^2\right] + \lambda\left\{2\left[\left(\frac{\partial U}{\partial X}\right)^2 + \left(\frac{\partial V}{\partial Y}\right)^2\right] + \left(\frac{\partial U}{\partial Y} + \frac{\partial V}{\partial X}\right)^2\right\} \tag{11}$$

Next, the irreversibility distribution ratio λ is defined as:

$$\lambda = \frac{\mu_{nf} T_0}{k_f}\left(\frac{\alpha_f}{L(T_H - T_C)}\right)^2 \tag{12}$$

The dimensionless total entropy generation, S_t is obtained by integrating equation (11) over the entire computational domain and hence is given by

$$S_t = \int S_{gen} dV \, . \tag{13}$$

2.2. Nanofluid thermophysical properties

The properties of the nanofluid can be defined on the basis of the properties of the pure liquid and solid nanoparticles. Following Ref. [11] these are defined as

$$\rho_{nf} = (1-\phi)\rho_f + \phi\rho_s \quad , \tag{14}$$

$$(\rho\beta)_{nf} = (1-\phi)(\rho\beta)_f + \phi(\rho\beta)_s \quad , \tag{15}$$

$$(\rho C_p)_{nf} = (1-\phi)(\rho C_p)_f + \phi(\rho C_p)_s \quad , \tag{16}$$

$$\alpha_{nf} = k_{nf} / (\rho C_p)_{nf} \quad , \tag{17}$$

$$\sigma_{nf} = (1-\phi)\sigma_f + \phi\sigma_s \quad , \tag{18}$$

Different factors can potentially influence the heat transfer enhancement of nanofluids and hence different models of nanofluids have been suggested. In a conventional approach, the effect of the particles Brownian motion is neglected due to the large particle size. As the particle size approaches nanometre scale, the particle Brownian motion and its effects on the surrounding liquids are magnified. The contribution of Brownian motion of nanoparticles with enhancement of thermal conduction could happen in two different ways: first, due to the movement of the nanoparticles, which can transfer the heat and second, through microconvection of the fluid around individual nanoparticles [62]. To consider these, the following models of viscosity and thermal conductivity are implemented.

The Brownian motion of the nanoparticles is taken into account by the method introduced in Ref. [54].

$$\mu_{nf} = \mu_{Static} + \mu_{Brownian} \quad . \tag{19}$$

In this equation μ_{Static} is the static viscosity calculated by Brickman equation [55], where

$$\mu_{Static} = \mu_f (1-\phi)^{-2.5} \quad , \tag{20}$$

and $\mu_{Brownian}$ is the viscosity due to Brownian motion of the nanoparticles and is expressed by

$$\mu_{Brownian} = 5\times10^4 \beta_n \phi \rho_f \sqrt{\frac{k_b T}{2\rho_s R_s}}\ f(T,\phi) \quad . \tag{21}$$

Following Ref. [56], thermal conductivities are defined as

$$k_{nf} = k_{Static} + k_{Brownian} \quad , \tag{22}$$

$$k_{Static} = k_f \left[\frac{\left(k_s + 2k_f\right) - 2\phi\left(k_f - k_s\right)}{\left(k_s + 2k_f\right) + \phi\left(k_f - k_s\right)} \right], \tag{23}$$

$$k_{Brownian} = 5\times10^4 \beta_n \phi \rho_f C_{p,f} \sqrt{\frac{k_b T}{2\rho_s R_s}}\ f(T,\phi)\ . \tag{24}$$

Also

$$k_b = 1.3807\times10^{-23}\ \ J/K$$
$$\beta_n = 0.0137(100\phi)^{-0.8229} \quad \text{for } \phi < 1\%$$
$$\beta_n = 0.0011(100\phi)^{-0.7272} \quad \text{for } \phi > 1\%$$
$$f(T,\phi) = \left(-6.04\phi + 0.4705\right)T + \left(1722.3\phi - 134.63\right)$$
$$\text{for } 1\% < \phi < 4\% \ \ \& 300K < T < 325K \tag{25}$$

In the Eq. (19), k_{Static} is the static thermal conductivity coefficient calculated through Maxwell's equation [57]. In Eq. (21), K_b is Boltzmann constant and β and f are modelling functions [56]. Table 1 shows the thermophysical properties of the investigated water and CuO nanofluid. In the proceeding calculations the numerical value of Prandtl number of water is considered to be 6.2.

2.3. Numerical scheme and validations

The governing Eqs. (1) - (4) with the corresponding boundary conditions given in Eq. (7) are solved using an in-house code developed on the basis of control volume formulation and SIMPLE algorithm [58]. The convection–diffusion terms are discretised by a power-law scheme and the system is numerically modelled in FORTRAN. A regular rectangular domain with a uniform grid is implemented. The following convergence criterion is considered.

$$\sum_j \sum_i \sqrt{\left(\frac{\gamma^{n+1} - \gamma^n}{\gamma^{n+1}}\right)^2} \le 10^{-7} \tag{26}$$

in which, n is the number of repetitions and γ stands for the non-dimensional parameters U, V and θ.

To verify the solution method and ensure the accuracy of the developed code, the numerical results were compared with those found in the literature. First, the results of natural convection in a differentially heated square enclosure obtained from the developed code was compared against the bench-mark solution of Davis [59]. Table 2 shows the outcomes of this comparison indicating negligible differences between the two Nusselt number groups. A square enclosure filled with water-CuO nanofluid featuring a heat source on the wall was previously modelled [60]. Figure 2 shows a comparison between the predictions of the developed numerical tool and those reported in Ref. [60]. Evidently, the two computations agree closely. In the next step, the accuracy of the code in modelling magnetohydrodynamic effects was evaluated. This assessment was carried out by comparing the results of the study of Pirmohammadi and Ghasemi [61]. These authors considered a two-dimensional, square enclosure in which two opposing walls were maintained at different constant temperatures and the other two walls were thermally insulated. Figure 3 shows the variation of Nu_m along the hot wall with a varying angle of the magnetic field calculated at three different Hartmann numbers. Clearly, the outputs of the

developed code feature a good agreement with the results of Pirmohammadi and Ghasemi [62]. In the final step, the effect of grid resolution was examined in order to select the appropriate grid density. Figures 4 shows the effect of the number of grid points on the average Nusselt number and the maximum value of stream function. This figure indicates that a 100 × 100 uniform grid can be used in the computations. The discussions presented in this sub-section serve as the full validation of the numerical simulations in the current study.

3. Results and discussion

The main objective of this investigation is to understand the influences of an I-shape enclosure upon the magnetohydrodynamics, natural convection of heat and generation of entropy of a nanofluid. Towards this aim, the computational tool developed and validated in section 2 is used in this section to conduct parametric studies. A large parametric space including Rayleigh number ($10^3 \leq \mathrm{Ra} \leq 10^6$), Hartmann number ($0 \leq Ha \leq 80$) and the nanoparticles volume fraction ($0 \leq \phi \leq 0.04$) is investigated. Further, the geometrical parameters of the enclosure are varied and the resultant modifications are analysed.

3.1 Effects of Rayleigh and Hartmann numbers and nanoparticles volume fraction

In this subsection the effects of Rayleigh number Hartmann number and nanoparticles volume fraction are investigated for fixed values of the enclosure geometric parameters (A=0.4 & B=0.4 in Fig.1). Figure 5 shows the streamlines for the nanofluid and pure water at different Rayleigh and Hartmann numbers. The buoyancy-driven circulating flows within the enclosure are evident for all investigated values of Rayleigh and Hartmann numbers. As expected, by increasing the value of Rayleigh number, the intensity of buoyancy forces and hence the maximum value of stream functions increases. Further, the streamlines are expanded throughout the enclosure, which is a clear indication of an increase in convection. Nevertheless, it is observed that the maximum value of stream function for the nanofluid is smaller than that of pure fluid. This could be attributed to the higher viscosity of nanofluid compared to the pure fluid, which slightly slows the flow. Figure 5 also shows that by intensifying the strength of the magnetic field, streamlines become symmetrical and the maximum flow velocity reduces. This can be readily verified by comparing the streamline patterns for Ra=10^4 and Ha=0 and those with the same Rayleigh number and nonzero values of Ha. In the absence of any magnetic field, the flow pattern inside the enclosure is noticeably asymmetric. This behaviour persists for both pure water and nanofluid. However, addition of the magnetic effect totally removes the asymmetric pattern. Interestingly, this organsing effect becomes less noticeable at higher Rayleigh numbers. That is such that for moderate values of Ha and Ra of 10^5 and 10^6 some deviation from symmetric flow pattern is observed. Regardless of the magnitude of Rayleigh number, this deviation significantly decreases at high values of Hartmann number (Ha=80) and the flow becomes almost perfectly symmetric. Figure 5, therefore, implies the opposing effects of Ra and Ha. The former generates a convection current in a complex and asymmetric way, while the latter attempts to organise the flow and maintain the symmetry.

Figure 6 depicts the isotherms for the same cases investigated in Fig. 5. This figure shows that for Ha=0 and low Ra the pattern of isotherms is slightly asymmetric, which then becomes perfectly symmetric at finite values of Ha. At low values of Ra, the flow rate is relatively small and the heat transfer is dominated by conduction. Hence, the effect of magnetic field stands out rather clearly. Also, for Ra=10^4 the isotherms tend to be parallel to the hot and cold walls, which is once again an indication of a conduction dominated system.

However, as the Rayleigh number increases, the isotherms become complex and the population of them grows near the bottom right corner of the hot wall and the upper left corner of the cold wall. Magnetic field tends to suppress this behaviour and the density of isotherms decreases at Ha=80. Figures 5 and 6 indicate that at low Ra the geometrical, flow and thermal axes of symmetry are all identical and essentially coincide on the vertical axis passing through the centre of the enclosure. Interestingly, at high values of Ra, the geometric and flow axes of symmetry are still more and less the same. The intensity of magnetic field determines the extent of the difference between the two axes. Yet, high values of Ra significantly modify the thermal pattern of the system. This is such that the isotherms become almost diagonally symmetric and most of heat transfer occurs at the top and bottom cavities and less thermal activities are observed in the middle cavity. This trend can have pronounced effects upon the design of I-shape enclosures and distinguishes them from square cavities, in which there is no sharp thermal distinction along the lateral walls [60, 61].

It was observed in Fig. 5 that the magnetic field can significantly modify the flow pattern. In order to obtain a better understanding of the flow behaviour within the enclosure, the vertical velocities at the mid-section of the enclosure, Y=0.5, are plotted in Fig. 7a for the highest Ra and three values of Ha. It is observed that by augmenting the magnetic field the maximum vertical velocity is reduced. This is such that for the case Ha=80 convection has been significantly suppressed. It is therefore concluded that at high values of Hartman number the vertical exchange of mass in the cavity is quite small. This renders the middle cavity rather insignificant in the overall convection problem, which is in keeping with the arguments made earlier on Fig. 6. Reduction of Ra in Figs. 7b and 7c leads to an overall decrease in the vertical velocity for all values of Ha, while the qualitative trend remains mostly unchanged. Nonetheless, a close comparison of Fig. 7a with Figs. 7b and 7c shows that at high Ra the maximum and minimum points on the velocity profile are always located close to the walls. However, at lower values of Ra number, these locations take a distance from the lateral walls and are situated closer to the centre of the duct. This strong motion of the fluid in the vicinity of the walls and the subsequent formation of boundary layer acts as a convective agent in the middle cavity. However, as shown in Fig. 6, the resultant heat transfer capability is still significantly lower than that of the top and bottom cavities. This is due to the fact that the rotation of the flow in the corners highly enhances the convection process near the sharp edges of the investigated geometry.

The values of average Nusselt number calculated on the hot walls for varying values of Ra, Ha and ϕ are given in Table 3. It is clear from this table that for high Rayleigh numbers there are higher average Nusselt numbers. In general, by increasing the volume fraction of nanoparticles the Nusselt number increases. This observation is in complete agreement with those reported in other geometries [9,26,38]. However, at Ra=10^5 and 10^6 a different behaviour is observed in which for $\phi \geq 0.02$ increasing ϕ results in a slight reduction of the Nusselt number. This can be explained by noting that at higher Ra the bulk motion of the fluid is rather significant. Through increasing the concentration of nanoparticles the viscosity of nanofluid increases. As shown in Fig. 5, this can impede the convection process and result in the reduction of Nusselt number. It is speculated that the multiple flow rotations and the induced strong shear stress in an I-shape enclosure magnify the influence of nanofluid viscosity upon the convection process. Table 3 also shows that the average Nusselt number decreases through increasing Ha. These declines are more obvious at Ra=10^5 and 10^6, in which convection is the dominant mechanism of heat transfer and, once again, are in keeping with the literature [33-36].

Figure 8 shows the variation of Nusselt number ratio, defined as $Nu_m^{**} = Nu_m/Nu_{m,\ \phi=0}$, against the nanoparticles volumetric concentration ($0 \le \phi \le 0.04$) for different values of Rayleigh number. This figure shows that, regardless of the value of Rayleigh number, nanofluid always features a greater Nusselt number compared to pure water. It is clear from Fig. 8 that addition of 1% nanoparticles results in a considerable increase in Nusselt number ratio. The figure also reflects a clear Rayleigh number dependent trend, wherein the Nu_m^{**} graph bifurcates into two branches. The first branch corresponds to the lower values of Rayleigh number (Ra=10^3 and 10^4) showing a monotonic increase of Nu_m^{**} with respect to the concentration of nanoparticles. The largest growth in Nusselt number ratio belongs to the lowest investigated concentration of nanoparticles, ϕ=0.01, while at higher concentrations the heat transfer enhancement is less significant. This branch includes weak convection or conduction dominated heat transfer processes. Under this condition, the increase in nanoparticles concentration and the resultant augmentation of the fluid thermal conductivity improve the heat transfer in comparison with that of pure fluid. The second or lower branch in Fig. 8, related to high Ra, shows a very different behaviour. Here, Nu_m^{**} increases with ϕ at low concentration. However, it starts to slightly decrease for higher values of nanoparticle concentration. This behaviour has been already discussed with regard to Table 3 and is due to the viscous effects of nanofluid at strong convective modes. It implies that at higher values of Ra there exists an optimal value of nanoparticle concentration, which will be a function of Rayleigh and Hartmann numbers. Clearly, finding this optimal concentration of nanoparticles is of engineering significance.

The effect of nanoparticles volume fraction percentage on entropy generation for Ha= 0 and 40 has been shown in Fig. 9. It is observed that with increasing the volume fraction of nanoparticles entropy generation rises slightly. This behaviour is consistent with that reported in the literature for other configurations and hence is not further discussed here. The effects of Hartmann number on heat transfer rate are investigated in Figure 10. This figure depicts the variation of average Nusselt number ratio, defined as $Nu_m^{*} = Nu_m/Nu_{m,\ Ha=0}$, with Hartmann number for different concentrations of nanoparticles and Rayleigh number. Figure 10 indicates that at low values of Rayleigh, wherein heat transfer is essentially through conduction, the magnetic field does not impart any major effect on the heat transfer process. Thus the average Nusselt number ratio remains nearly unchanged or features only minor declines when Hartmann number increases. For higher values of Rayleigh number, however, the average Nusselt number ratio decreases significantly by increasing the Hartmann number. This is observed in the cases for which heat transfer is mainly due to convection and the magnetic field can suppress the fluid motion and weaken the heat convection.

In Fig.11 the profiles of total entropy generation against Hartmann Number are presented for different values of Ra. This figure shows that, in general, with increasing the intensity of the magnetic field, entropy generation decreased. However, the extent of this decrease is negligible for Ra=10^3 and 10^4 for which convection is quite weak and heat transfer is conduction dominated. Yet, it becomes more noticeable at Ra= 10^5, 10^6 wherein convection dominates the heat transfer process.

Figures 12 illustrates the effects of Hartmann number on the average Nusselt numbers evaluated at different parts of the hot wall for Ra=10^4 and 10^6. The left side of the I-shape enclosure has been divided into five flat walls as specified in the subset of Fig. 12 and the average Nusselt number (see Eq. 9) was calculated on each wall. Figure 12a shows that at low Ra the highest heat transfer rate belongs to the wall of the middle cavity, denoted by S_3 in this figure. All other walls have significantly lower Nusselt numbers. This behaviour could be readily explained by noting that for low Rayleigh number heat transfer is essentially by conduction and

S_3 is the closet wall to the cold side of the configuration. As a result, the thermal resistance associated with heat conduction on this wall is minimal and its heat transfer rate is the largest amongst all surfaces. As discussed earlier, application of the magnetic field in this case, generally, results in a small reduction of the heat transfer rate. Nonetheless, Fig. 12a shows that there are two exceptions to this general trend, in which surfaces S_4 and S_5 feature a slight increase in Nusselt number at finite values of Hartmann number. This local increase in the Nusselt number can be explained by referring to the streamline patterns in Fig. 5. This figure shows that at low Ra and in the absence of magnetic effects there is a weak natural convection flow from the bottom left to the top right corner of the enclosure. Hence, for Ha=0 the top left corner (S_5 and S_4) are not in contact with any noticeably moving fluid and heat transfer from them is purely conductive. Application of the magnetic field tends to organise the flow around the vertical axis (see Fig. 5) and therefore at Ha=40 there exists a vortex in the vicinity of S_5 and S_4. The introduction of bulk fluid motion increases the rate of heat transfer on these two surface and results in the augmentation of Nusselt number. Further increase in Ha brings the vortex closer to the surfaces. Yet, it makes the flow slower and thus the gain in the Nusselt numbers of S_5 and S_4 becomes quite small at higher Hartmann numbers. It is noted that all other investigated surfaces in Fig. 12a are initially in contact with convection currents. These are then retarded by the magnetic field, which leads to the reduction of the Nusselt number on those surfaces. It is, also, noted that at high values of Ha the surfaces on the top and bottom of the enclosure show very similar Nusselt number (compare Nusselt numbers for S_1 and S_2 with those for S_5 and S_4 in Fig. 12a). This is due to the fact that at high Ha the fluid motion and therefore natural convection is significantly suppressed. The system is, therefore, mainly conductive and the distance between the hot and cold surfaces is the main parameter dominating the rate of heat transfer.

Increase of Rayleigh number in Fig. 12b results in very pronounced increases in the Nusselt number of all surfaces. It also causes more noticeable reductions of Nusselt number at higher Hartmann number for some surfaces. It is inferred from Fig. 12b that the heat transfer at high Rayleigh and low Hartmann number is dominated by that of surface S_1 (the bottom corner). This is consistent with the flow and thermal patterns shown in Figs. 5 and 6, in which there is a strong convection current near this surface. Interestingly, addition of the magnetic field decreases the share of surface S_1 in the overall heat transfer process and at high Hartmann numbers the contributions of surfaces S_1, S_2 and S_3 are quite comparable. The observed major surface dependency of heat transfer at varying Rayleigh and Hartmann numbers has strong implications in the design of enclosures. It highlights the significance of considering the precise geometry of the enclosure and the considerable errors associated with approximating an I-shape cavity with a square shape or any other configuration.

3.2 Effect of geometrical parameters

Figure 13 shows the influences of varying the geometrical parameters *A* and *B* (as defined by Eq. 5) upon the pattern of streamlines and isotherms. It is clear from this figure that changes in the geometry can lead to the development of a wide variety of hydrodynamic and thermal patterns. In the case of A=0.4 and B=0.8, the I-shape enclosure approaches the classical square enclosure and the pattern of streamlines and isotherms resemble those of square cavities [14,15,30]. Moving to the cases of A=0.4 and B=0.2 and also that with A=0.2 and B=0.4 changes the patterns considerably and makes them similar to those discussed in Figs. 5 and 6. However, the case of A=0.8 and B=0.4 shows a radically different behaviour, in which there is nearly no flow or heat transfer

within the top and bottom flaps. The flow in this case is limited to a central convection roll in the middle section of the enclosure and there exists strong heat transfer at the top and bottom corners of this part.

Figure 14 shows variation of the average Nusselt number with respect to the geometrical parameter *A* for three different values of Rayleigh number. Referring to the problem configuration in Fig.1, as *A* increases, the enclosure flaps become narrower. Figure 13 showed that in this case convection decreases proportionally and hence the average Nusselt number decreases. At $Ra=10^4$, a mild descending trend in Nusselt number with respect to *A* is observed. Figure 14 shows that by increasing the Rayleigh number to 10^5 there are only marginal modifications of the qualitative and quantitative behaviours of Nu compared to that at $Ra=10^4$. However, increasing Ra to 10^6 increases the Nusselt number substantially and makes it much more sensitive to variations in *A*. Figure 14, once again, demonstrates the significant influences of the enclosure geometry upon the heat transfer and thermal response of the system to the applied magnetic field. The effects of variations in the height of the middle section or parameter *B* are investigated in Fig. 15. A comparison between Fig. 15 and Fig. 14 indicates that the influences of parameters *A* and *B* are rather different. An increase in *B* has relatively small effects on the Nusselt number at high values of Rayleigh number, whereas it considerably reduces the Nusselt number at lower Rayleigh numbers. Figure 16 shows the effects of geometric parameters *A* on the total generation of entropy. It is observed that with rising A, the total entropy generation increases monotonically for $Ra=10^4$. This is analogous to the behaviour of average Nusselt number with respect to *B* for the same Rayleigh number, shown in Fig. 15. Interestingly, the monotonic trend changes at higher values of Rayleigh number and extremum points appear in the graphs of total entropy at $Ra=10^5$ and $Ra=10^6$ of Fig. 16. This implies that there exist certain shapes of the enclosure for which the irreversibility of the system is minimal. The effects of geometric parameters *B* on the total generation of entropy are shown in Fig.17. It is observed that with rising *B* the total entropy generation decreases monotonically for all investigated values of Ra. This is distinctive to the variations of total entropy with respect to *A*, in which extremum points appear in the total entropy graphs. It indicates the dissimilar effects of geometrical parameters and hence highlights the importance of considering the exact geometry in the second law analyses of enclosures.

4. Conclusions

Magnetohydrodynamics and natural convection of heat in an I-shape enclosure filled with a nanofluid were investigated numerically for the first time in the literature. A computational code was developed and rigorously validated against a number of previous studies on other configurations. Brownian motion of the nanoparticles and their induced viscosity and thermal conductivity were numerically modelled. In keeping with other investigations in the field of magnetohydrodynamics, it was observed that application of a magnetic field retards the flow and therefore suppresses the overall heat transfer process. The specific findings of the analyses conducted in this paper can be summarised as follows.

- At low Rayleigh numbers, where heat transfer is conduction dominated, application of magnetic field results in developing an almost perfectly symmetric pattern of streamlines and isotherms. Nevertheless, the organising effect of the magnetic field reduces as the Rayleigh number increases.
- The hydrodynamics and heat transfer within the I-shaped enclosure were found strongly dependent upon the geometry. At high Rayleigh numbers, strong asymmetric rotating flows develop near the corners of the enclosures.

- Similar to the findings of the existing studies on other configurations, it was observed that, in general, increasing Ha results in the reduction of the average Nusselt number.
- As a crucial peculiarity of the investigated configuration, it was found that there is a significant variation in the numerical value of Nusselt numbers calculated on the different surfaces of the enclosure. These Nusselt numbers also feature different levels of Hartmann number sensitivity.
- At low and moderate Rayleigh numbers, increasing the concentration of nanoparticles always results in augmentation of the Nusselt numbers. Yet, at high Rayleigh numbers, with strong convection currents, there is a small drift of Nusselt number after exceeding an optimal value of nanoparticle concentration. It was argued that this is due to the organising effects of the magnetic field in the I-shape enclosure.
- It was shown that geometrical specifications of the I-shape enclosures can significantly modify the rate of heat transfer.
- The entropy generation decreases with the applied magnetic field and raises with increasing nano-particles. Variations in the geometrical parameters of the enclosure can minimise the total generation of entropy.

The results presented in this paper clearly showed the significance of considering the exact configuration of the enclosure in thermal design of nanofluid filled cooling systems. In particular, they indicate that approximating an I-shape enclosure with a square cavity could result in large error margins. The physical insights developed in this study remain transferable to more sophisticated turbulent cases when very high Rayleigh numbers are considered.

References

[1] R. B. Schoch, J. Han and P. Renaud, Transport phenomena in nanofluids, Reviews of Modern Physics 80 (2008) 839.

[2] L. B. Godson, D. Raja, M. Lal and S. Wongwises, Enhancement of heat transfer using nanofluids-an overview, Renewable and Sustainable Energy Reviews 14 (2010) 629-641.

[3] E. Efstathios and S. Michaelides, Nanofluidics- Thermodynamic and Transport Properties, Springer International Publishing, Switzerland 2014.

[4] P. Vadasz, Heat conduction in nanofluid suspensions, J. Heat Transfer 128 (2006) 465-477.

[5] M. Torabi, C. Dickson, N. Karimi, Theoretical investigation of entropy generation and heat transfer by forced convection of copper-water nanofluid in a porous channel- Local thermal non-equilibrium and partial filling effects, J. Powder Tech. 301(2016) 234-254.

[6] C. Dickson, M. Torabi, N. Karimi, First and second law analysis of nanofluid convection through a porous channel-The effects of partial filling and internal heat sources, J. Applied Thermal Engineering 103(2016) 459–480.

[7] M. Torabi, K. Zhang, N. Karimi, G. P. Peterson, Entropy generation in thermal systems with solid structures-a concise review, Int. J. Heat and Mass Transfer 97(2016) 917-931.

[8] O. Mahian, A. Kainifar, S. A. Kalogirou, I. Pop and S. Wongwises, A review of the applications of nanofluids in solar energy, Int. J. Heat and Mass Transfer 57(2013) 582-594.

[9] M. Lomascolo, G. Colangelo, M. Milanese and A. De Risi, Review of heat transfer in nanofluids: Conductive, convective and radiative experimental results, Renewable and Sustainable Energy Reviews

43(2015)1182-1198.

[10] Ebrahimi, Khosrow, Gerard F. Jones, and Amy S. Fleischer. A review of data center cooling technology, operating conditions and the corresponding low-grade waste heat recovery opportunities. J. Renewable and Sustainable Energy Reviews 31(2014)622-638.

[11] B. Ghasemi , S.M. Aminossadati , Brownian motion of nanoparticles in a triangular enclosure with natural convection, Int. J. Thermal Sci. 49(2010) 931-940

[12] K. Khanafer, K. Vafai, M. Lightstone, Buoyancy-driven heat transfer enhancement in a two-dimensional enclosure utilizing nanofluids , Int. J. Heat and Mass Transfer 46(2003) 3639, 2003.

[13] GH.R. Kefayati , S.F. Hosseinizadeh, M. Gorji, H. Sajjadi, Lattice Boltzmann simulation of natural convection in tall enclosures using water/SiO2 nanofluid , Int. Commun. in Heat and Mass Transfer 38(2011)798–805.

[14] F.H. Lai,Y. Yang, Lattice Boltzmann simulation of natural convection heat transfer of Al2O3/water nanofluids in a square enclosure, Int. J. Thermal Sci. 50(2011)1930-1941.

[15] A.H. Mahmoudi , M. Shahi, A.H. Raouf, A. Ghasemian , Numerical study of natural convection cooling of horizontal heat source mounted in a square cavity filled with nanofluid, Int. Commun. In Heat and Mass Transfer 37(2010) 1135–1141.

[16] S. Chandrasekhar, Hydrodynamic and hydromagnetic stability. Courier Corporation 2013.

[17] M.A.A. Hamad, I. Pop, A. I. M. Ismail, Magnetic Field Effects on Free Convection Flow of a Nanofluid Past a Vertical Semi-Infinite Flat Plate, Nonlinear Analysis: Real World Applications 12 (2011) 1338–1346.

[18] A. Gavili, F. Zabihi, T.D. Isfahani, J. Sabbaghzadeh, The Thermal Conductivity of Water Base Ferrofluids Under Magnetic Field, Exp. Thermal and Fluid Sci.41(2012) 94–98.

[19] T. Hayat, M. Waqas, S. A. Shehzad, A. Alsaedi, A model of solar radiation and Joule heating in magnetohydrodynamic (MHD) convective flow of thixotropic nanofluid, J. Molecular Liquids 215(2016) 704-710.

[20] F. Guerrero Martinez, P. Younger, N. Karimi, S. Kyriakis, Three-dimensional numerical simulations of free convection in a layered porous enclosure, Int. J. Heat and Mass Transfer 106(2017)1005-1013. DOI dx.doi.org/10.1016/j.ijheatmasstransfer.2016.10.072

[21] H.R. Ashorynejad, A.A. Mohamad M. Sheikholeslami, Magnetic field effects on natural convection flow of a nanofluid in a horizontal cylindrical annulus using Lattice Boltzmann method, Int. J. Thermal Sci., 64(2013) :240-250.

[22] W.M. Rohsenow, J.P. Hartnett,Y.I. Cho, Handbook of heat transfer. Third ed., McGraw-Hill, New York 1998.

[23] GH.R. Kefayati, Lattice Boltzmann simulation of MHD natural convection in a nanofluid-filled cavity with sinusoidal temperature distribution, Powder Technol. 243 (2013)171–83.

[24] GH.R Kefayati, FDLBM simulation of entropy generation due to natural convection in an enclosure filled with non-Newtonian nanofluid, Powder Technol. 273 (2015) 176–90.

[25] GH.R. Kefayati, FDLBM simulation of mixed convection in a lid-driven cavity filled with non-Newtonian nanofluid in the presence of magnetic field, Int. J. Thermal. Sci. 95(2015)29–46.

[26] M. Sheikholeslami, D.D. Ganji, Nanofluid convective heat transfer using semi analytical and numerical approaches: a review, J.Taiwan Institute of Chemical Engineers 65(2016) 43-77.

[27] K. Sanokawa, Natural Confection of Mercury in a Magnetic Field parallel to the. Gravity, J. Heat Transfer 101 (1979) 227-232.

[28] O. Hiroyuki, K. Okada, The effect of the direction of the external magnetic field on the three-dimensional natural convection in a cubical enclosure, Int. J. Heat and Mass Transfer 32.10 (1989) 1939-1954.

[29] N. Rudraiah, Effect of a magnetic field on free convection in a rectangular enclosure." Int. J. Engineering Science 33.8 (1995) 1075-1084.

[30] M. Pirmohammadi, M. Ghassemi, M. Hamedi, Effect of inclination angle on magneto-convection inside a tilted enclosure, IEEE transactions on magnetics 46.6 (2010) 2489-2492.

[31] A.J. Chamkha, Hydromagnetic combined convection flow in a vertical lid-driven cavity with internal heat generation or absorption, Numerical Heat Transfer- Part A: Applications 41.5 (2002) 529-546.

[32] F. Guerrero Martinez, P. Younger, N. Karimi, Three-dimensional numerical model of free convection in sloping porous enclosures, Int. J. Heat and Mass Transfer 98(2016)257-267, Doi: 10.1016/j.ijheatmasstransfer.2016.03.029.

[33] M. Sheikholeslami, M. Gorji-Bandpy, D.D. Ganji, S. Soleimani, Natural convection heat transfer in a cavity with sinusoidal wall filled with CuO–water nanofluid in presence of magnetic field, J. Taiwan Institute Chemical Engineering 45(2014)40–49.

[34] B. Ghasemi, S.M. Aminossadati , A. Raisi, Magnetic field effect on natural convection in nanofluid- filled square enclosure, Int. J. Thermal Sci. 50(2011) 1748-1756.

[35] M. Sheikholeslami, M. Gorji-Bandpy, D.D. Ganji, S. Soleimani, MHD natural convection in a nanofluid filled inclined enclosure with sinusoidal wall using CVFEM, Neural Comput. Appl. 24 (2014) 873–82.

[36] R. Alizadeh, N. Karimi, R. Arjmandzadeh, A. Mehdizadeh, Mixed convection and thermodynamic irreversibilities in MHD nanofluid stagnation-point flows over a cylinder embedded in porous media, J. Thermal Analysis and Calorimetry (2018), doi: 10.1007/s10973-018-7071-8.

[37] M. Turkyilmazoglu, Performance of direct absorption solar collector with nanofluid mixture, Energy Conversion and Management 114 (2016) 1-10.

[38] M. Turkyilmazoglu, Condensation of laminar film over curved vertical walls using single and two-phase nanofluid models, European J. Mechanics-B/Fluids 65 (2017) 184-191.

[39] M. Turkyilmazoglu, Magnetohydrodynamic two-phase dusty fluid flow and heat model over deforming isothermal surfaces, Physics of Fluids 29.1 (2017) 013302.

[40] R. Cortell, A note on magnetohydrodynamic flow of a power-law fluid over a stretching sheet, Applied Mathematics and Computation 168.1 (2005) 557-566.

[41] T. Fang, J. Zhang, S. Yao, Slip MHD viscous flow over a stretching sheet–an exact solution, Commun. in Nonlinear Science and Numerical Simulation 14.11 (2009) 3731-3737.

[42] A. Bejan, A study of entropy generation in fundamental convective heat transfer, ASME J. Heat Transfer 101 (1979) 718–725.

[43] A. Bejan, Entropy Generation through Heat and Fluid Flow, Wiley, New York,1982.

[44] A. Bejan, Entropy Generation Minimization: The Method of Thermodynamic Optimization of Finite-Size Systems and Finite-Time Processes, CRC Press, Boca Raton, 1996.

[45] N. Hajialigal, A. Fattahi, M. H. Ahmadi, M. E. Qomi, and E. Kakoli,, MHD mixed convection and entropy generation in a 3-D microchannel using Al2O3-water nanouid, Taiwan Institute of Chemical Engineers, 46 (2015) 30-42.

[46] Z. Mehrez, A. E. Cafsi, A. Belghith, and P. L. Quere, MHD effects on heat transfer and entropy generation of nanofluid flow in an open cavity, J. Magnetism and Magnetic Materials, 374(2015) 214-224.

[47] G.H.R. Kefayati, Nor Azwadi Che Sidik, Simulation of natural convection and entropy generation of non-newtonian nanofluid in an inclined cavity using buongiorno's mathematical model (part ii, entropy generation), Powder Technol. 305 (2017) 679–703.

[48] I. Fersadou, H. Kahalerras, M. El Ganaoui, MHD mixed convection and entropy generation of a nanofluid in a vertical porous channel, Comp. Fluids 121 (2015) 164–179

[49] M.A. Sheremet, I. Pop, M.M. Rahman, Three-dimensional natural convection in a porous enclosure filled with a nanofluid using Buongiorno's mathematical model, Int. J. Heat and Mass Transfer 82 (2015) 396–405.

[50] HR. Ashorynejad , A.A. Mohamad, M. Sheikholeslami, Magnetic field effects on natural convection flow of a nanofluid in a horizontal cylindrical annulus using lattice Boltzmann method, Int. J. Thermal Sci. 64(2013) 240–50.

[51] R. Alizadeh, A. B. Rahimi, N. Karimi, A. Alizadeh, Transient analysis of the interactions between a heat transferring, radial stagnation flow and a rotating cylinder-Magnetohydrodynamic and non-uniform transpiration effects, J. Thermal Science and Engineering Applications 10(2018) 051017-1, doi:10.1115/1.4040363

[52] F. Guerrero Martinez, N. Karimi, Eduardo Ramos, Numerical modeling of multiple steady-state convective modes in tilted porous medium heated from below, Int. Communications in Heat and Mass Transfer 92(2018) 64-72.

[53] A. M Bouchoucha, R. Bessaïh, H. F. Oztop, K. Al-Salem, F. Bayrak, Natural convection and entropy generation in a nanofluid filled cavity with thick bottom wall: Effects of non-isothermal heating, Int. J. Mechanical Sciences, 2017.

[54] J. Koo, C. Kleinstreuer, Laminar nanofluid in microheat-sinks, Int. J. Heat and Mass Transfer 13 (2005) 2652-2661.

[55] H.C. Brinkman, The Viscosity of Concentrated Suspensions and Solution, Chem. Phys. 20 (1952) 571–581.

[56] J. Koo, C. Kleinstreuer, A new thermal conductivity model for nanofluids, J. Nanoparticle Research 6 (2004) 577-588.

[57] J. Maxwell, A Treatise on Electricity and Magnetism, second ed. Oxford University Press, Cambridge, UK, 1904.

[58] S.V. Patankar, Numerical Heat Transfer and Fluid Flow, Hemisphere, Washington D. C., 1980.

[59] G.D.V. Davis, Natural Convection of Air in a Square Cavity, a Benchmark Numerical Solution, Int. J. Numer. Meth. Fluid 3 (1983) 249–264.

[60] H.F. Oztop, E. Abu-Nada, Numerical Study of Natural Convection in Partially Heated Rectangular Enclosures Filled with Nanofluids , Int. J. Heat and Fluid Flow 29 (2008) 1326–1336.

[61] M. Pirmohammadi, M. Ghassemi, Effect of Magnetic Field on Convection Heat Transfer Inside a Tilted Square Enclosure ", Int. Commun. Heat and Mass Transfer 36 (2009)776–780.

[62] H. S. Aybar, M. Sharifpur, R. Azizian, M. Mehrabi, J. P. Meyer, A Review Of Thermal Conductivity Models for Nanofluids, J. Heat Transfer Engineering 36(2015) 1085-1110.

Table Caption

Table 1. Thermophysical properties of pure water and CuO [11]

Table 2. Comparison between the simulations of the developed code and those reported in Ref. [59]

Table 3. Variation of the average Nusselt number with different concentration of nanoparticles at varying Rayleigh and Hartmann numbers

Figure Caption

Fig.1: A schematic diagram of the physical model

Fig.2 : Comparison between the present simulations with that of Ref. [60] for square enclosure filled by nanofluid

Fig.3: Comparison of the present simulation with those of Ref. [61] for square enclosure under different rotation angles of the magnetic field

Fig.4: Grid independency study ($\phi = 0.04, \mathrm{Ha} = 40, \mathrm{Ra} = 10^5$)

Fig. 5: Streamlines for the enclosures filled with CuO–water nanofluid ϕ=0.04(– – –) and pure water (——) at different Rayleigh and Hartmann numbers.

Fig. 6: Isothermlines for the enclosures filled with CuO–water nanofluid ϕ=0.04(– – –) and pure water (——) at different Rayleigh and Hartmann numbers.

Fig. 7: Dimensionless vertical velocity profile at Y=0.5, ϕ=0.04, (a) Ra=10^6 ,(b) Ra=10^5 , (c) Ra=10^4

Fig. 8: Variation of average Nusselt number ratio with ϕ at Ha=40

Fig. 9: Variation of the Total Entropy generation with ϕ at (a) Ha=0 and (b) Ha=40

Fig. 10: Effect of Hartmann number on the variation of the average Nusselt number ratio for different nano-particle concentrations

Fig. 11: Effects of Hartmann number on the variation of the Total Entropy at ϕ=0.04

Fig. 12: Effect of Hartmann number on the local Nusselt number at, (a) Ra=10^4 and (b) Ra=10^6.

Fig. 13: Streamline (up) and isotherms (down). Ra=10^6, ϕ=0.04, Ha=40.

Fig. 14: Effect of variation of the distance of the enclosure flaps, *A*, on the average Nusselt number, ϕ=0.04, Ha=40.

Fig. 15: Effect of the connector of the enclosure (the web) thickness, *B*, on the average Nusselt number, ϕ=0.04, Ha=40.

Fig. 16: Effects of variations in the distance of the enclosure flaps, *A*, on the Total Entropy generation, ϕ=0.04, Ha=40 *B*= 0.4

Fig. 17: Effects of the thickness of enclosure connector, *B*, on the Total Entropy generation, ϕ=0.04, Ha=40, *A*= 0.4.

Table 1. Thermophysical properties of pure water and CuO [11].

	Pure water	CuO
ρ (kgm^{-3})	997.1	6320
C_p ($Jkg^{-1}K^{-1}$)	4179	531.8
k ($Wm^{-1}K^{-1}$)	0.613	76.5
$\times 10^{+5}$ (K^{-1})β	21	1.8

Table 2. Comparison between the simulations of the developed code and those reported in Ref. [59].

Ra	Nu_m (present work)	Nu_m (Davis [59])	Difference
10^3	1.110	1.116	0.54%
10^4	2.207	2.234	1.2%
10^5	4.524	4.503	0.53%
10^6	8.799	8.789	0.01%

Table 3. Variation of the average Nusselt number with different concentration of nanoparticles at varying Rayleigh and Hartmann numbers.

		ϕ=0	ϕ=0.01	ϕ=0.02	ϕ=0.03	ϕ=0.04
	Ha=0	5.244	6.30	6.48	6.564	6.597
$Ra=10^3$	Ha=40	5.236	6.293	6.473	6.558	6.591
	Ha=80	5.235	6.292	6.473	6.557	6.591
	Ha=0	5.792	6.782	6.928	6.982	6.988
$Ra=10^4$	Ha=40	5.296	6.343	6.518	6.598	6.628
	Ha=80	5.249	6.304	6.483	6.566	6.599
	Ha=0	11.747	13.167	13.252	13.198	13.072
$Ra=10^5$	Ha=40	7.97	8.895	8.918	8.853	8.747
	Ha=80	6.321	7.258	7.352	7.362	7.329
	Ha=0	27.424	30.794	31.006	30.888	30.599
$Ra=10^6$	Ha=40	22.957	25.464	25.43	25.14	21.724
	Ha=80	16.888	18.522	18.385	18.082	17.706

Figures:

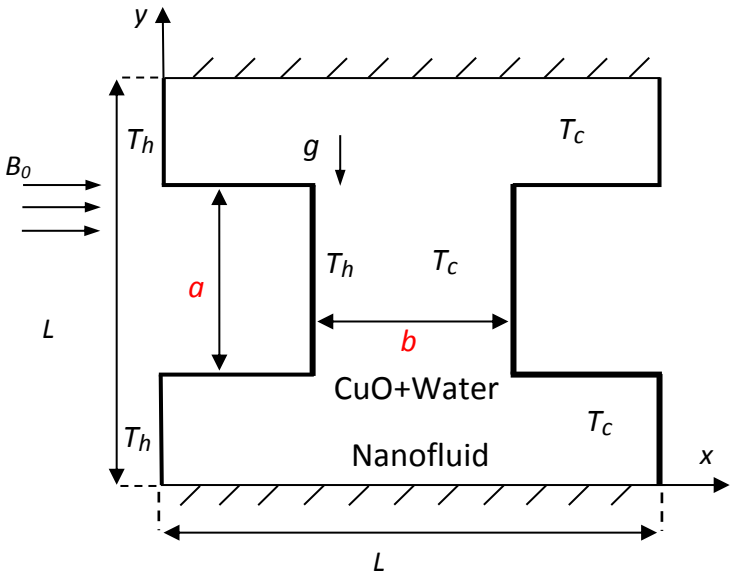

Fig.1: A schematic diagram of the physical model.

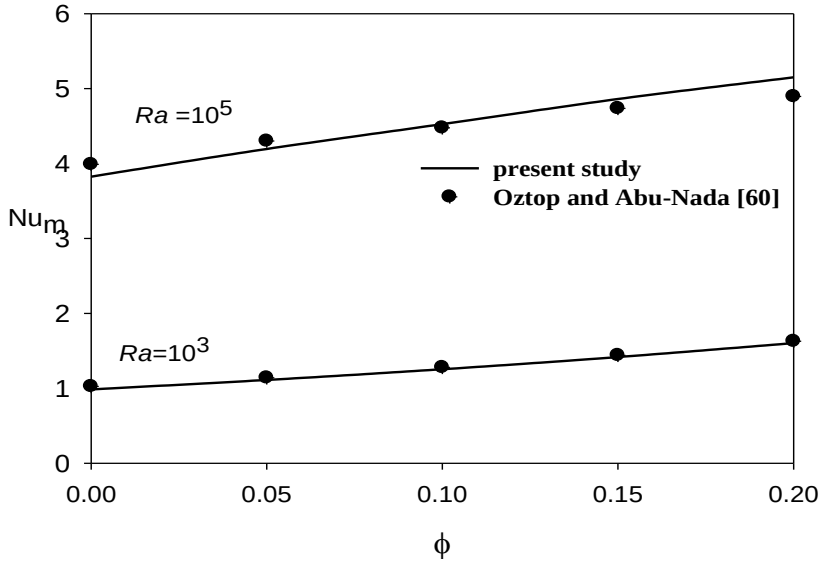

Fig. 2. Comparison between the present simulations with those of Ref. [60] for square enclosure filled by nanofluid.

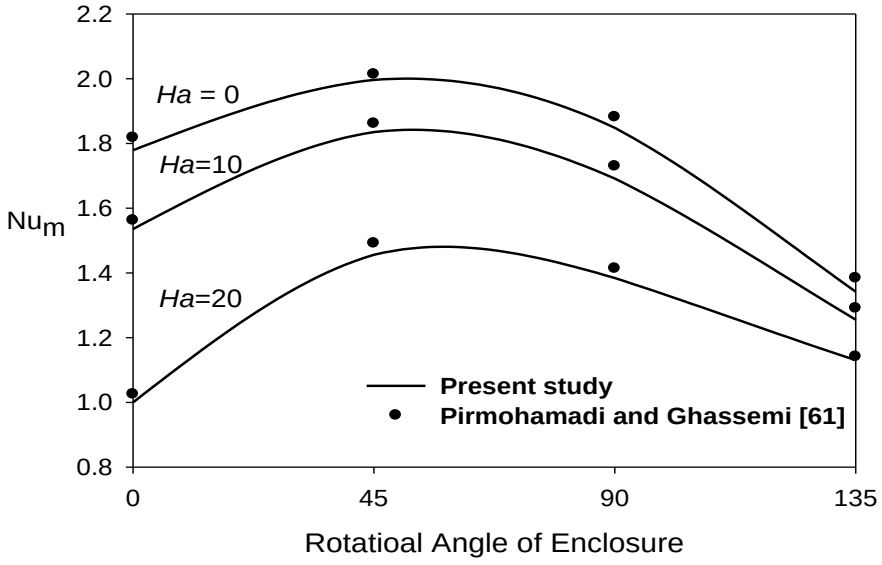

Fig.3. Comparison of the present simulation with those of Ref. [61] for square enclosure under different rotation angles of the magnetic field.

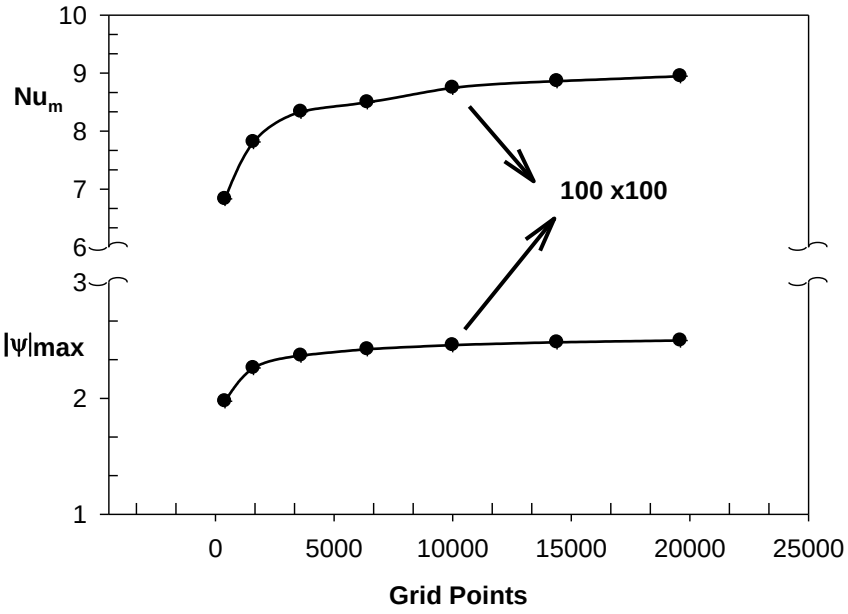

Fig. 4. Grid independency study ($\phi = 0.04, Ha = 40, Ra = 10^5$).

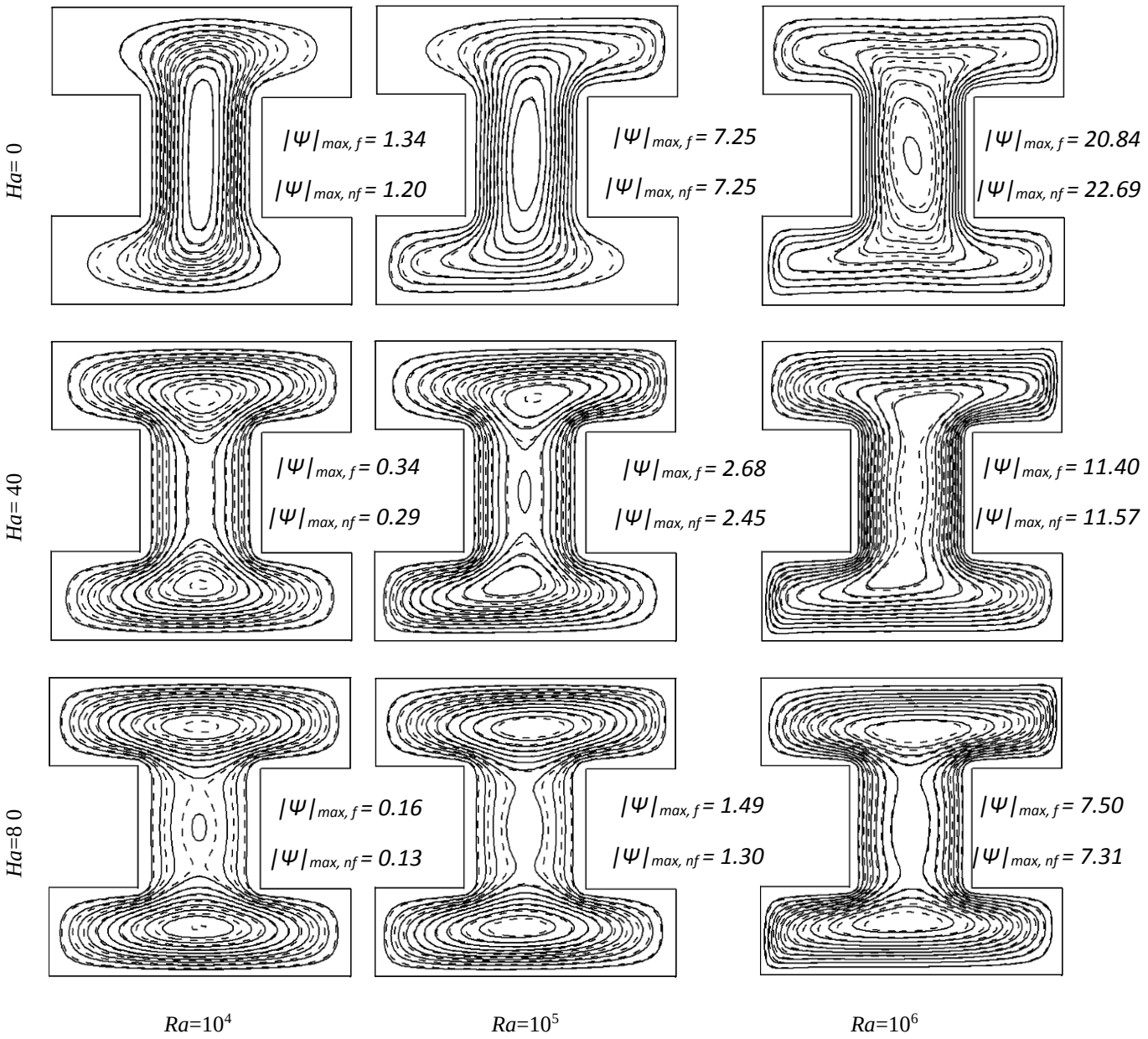

Fig. 5. Streamlines and the maximum values of steam functions for the enclosures filled with CuO–water nanofluid, ϕ=0.04(– – –) and pure water (——) at different Rayleigh and Hartmann numbers.

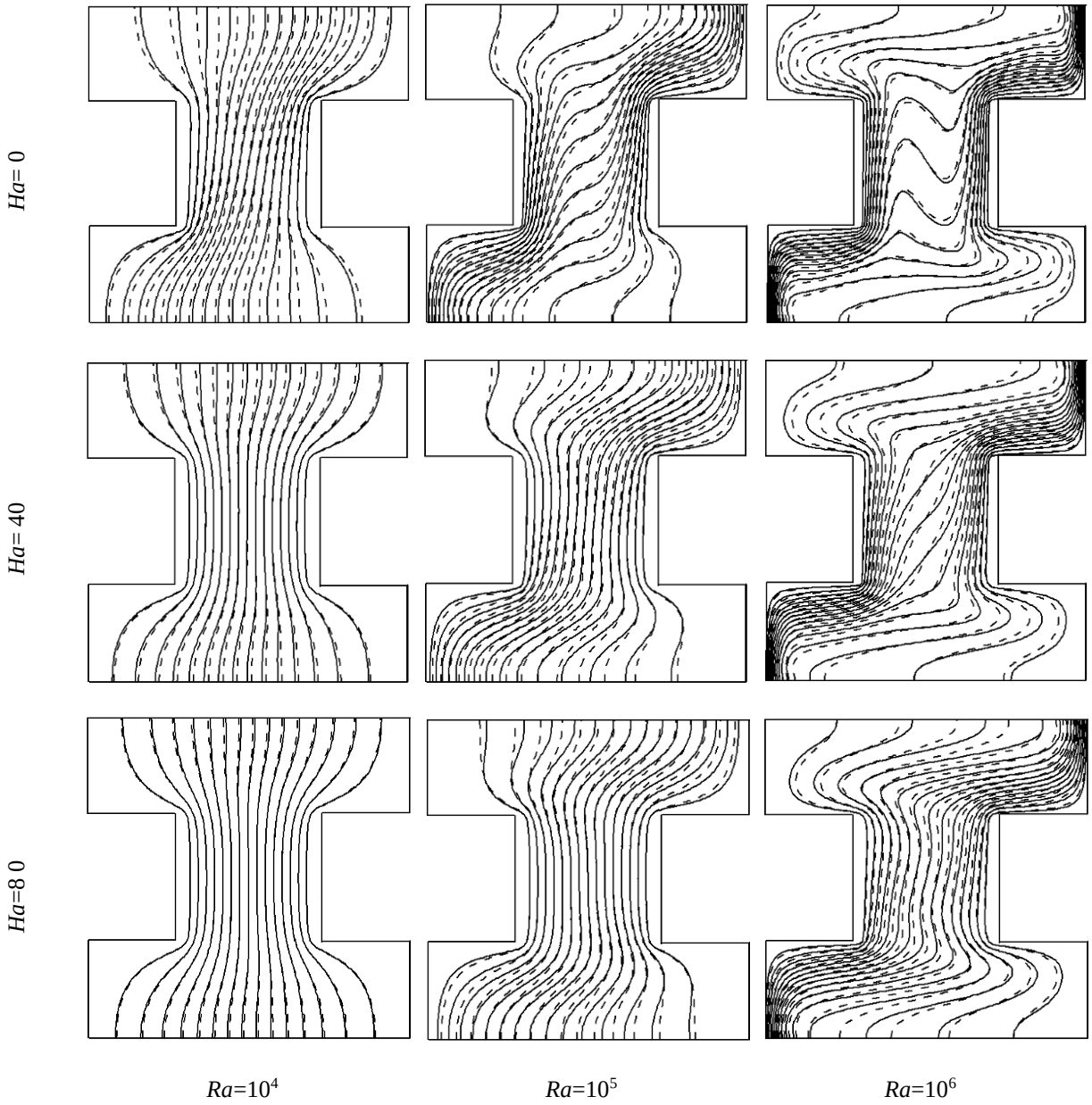

Fig. 6. Isotherm lines for the enclosures filled with CuO–water nanofluid, ϕ=0.04(– – –) and pure water (——) at different Rayleigh and Hartmann numbers.

(a)

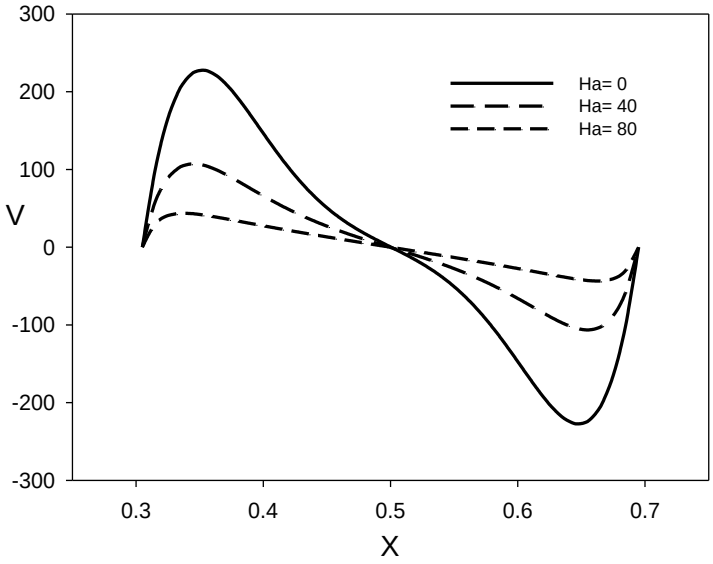
300
200
100
0
-100
-200
-300
V
0.3
0.4
0.5
0.6
0.7
X
Ha= 0
Ha= 40
Ha= 80

(b)

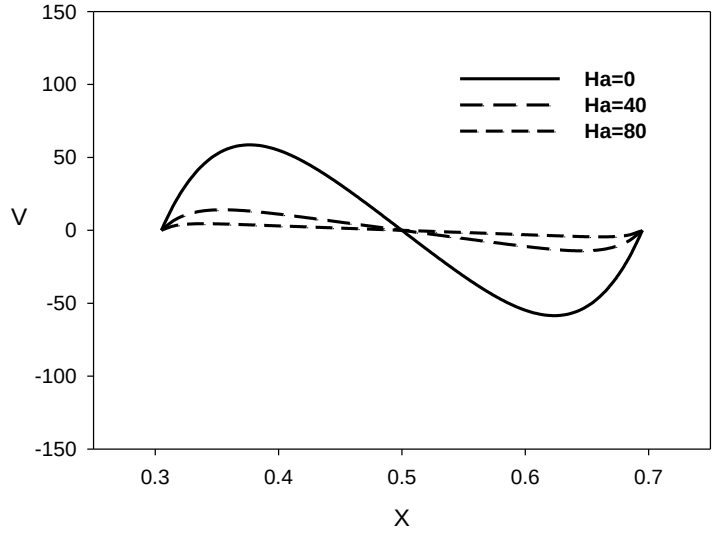
150
100
50
0
-50
-100
-150
V
0.3
0.4
0.5
0.6
0.7
X
Ha=0
Ha=40
Ha=80

(c)

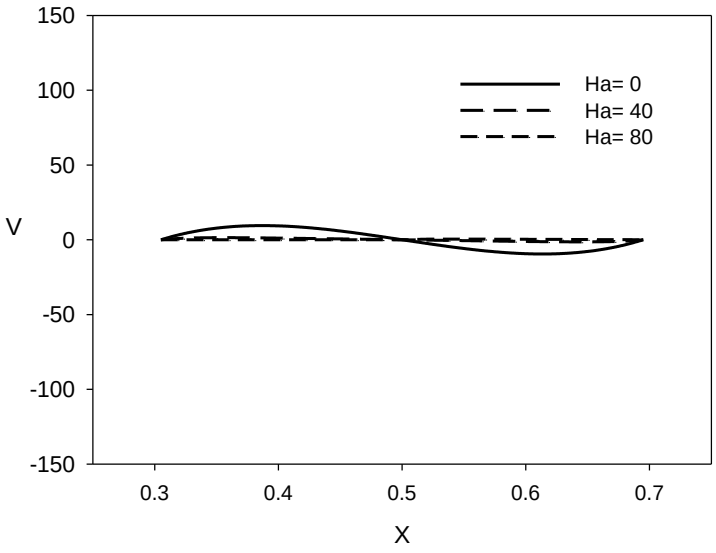

Fig. 7. Profiles of the dimensionless vertical velocity at Y=0.5, ϕ=0.04, (a) Ra=10^6 ,(b) Ra=10^5 , (c) Ra=10^4.

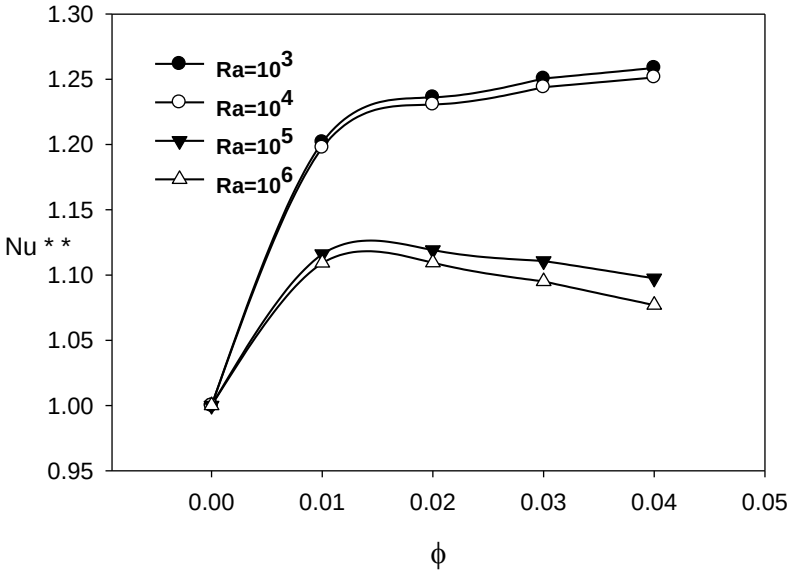

Fig. 8. Variation of the average Nusselt number ratio with ϕ at Ha=40.

a)

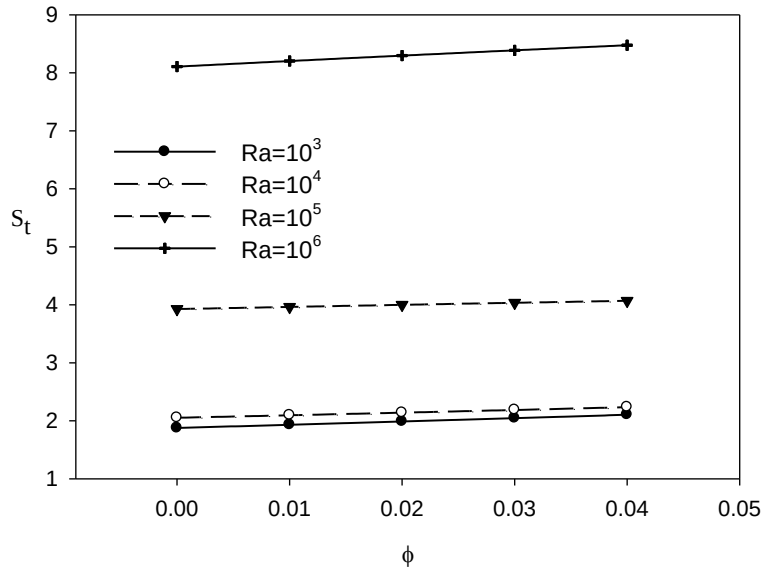

b)

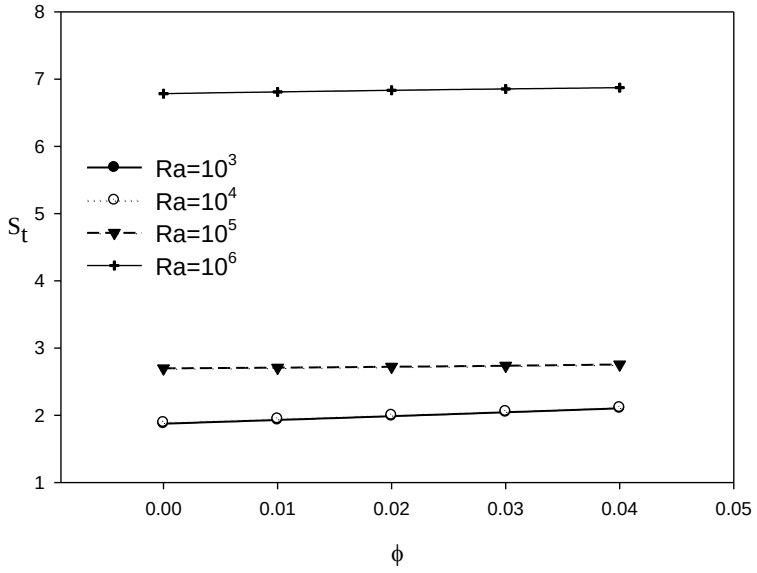

Fig. 9 Variation of the Total Entropy generation with ϕ at (a) Ha=0 and (b) Ha=40.

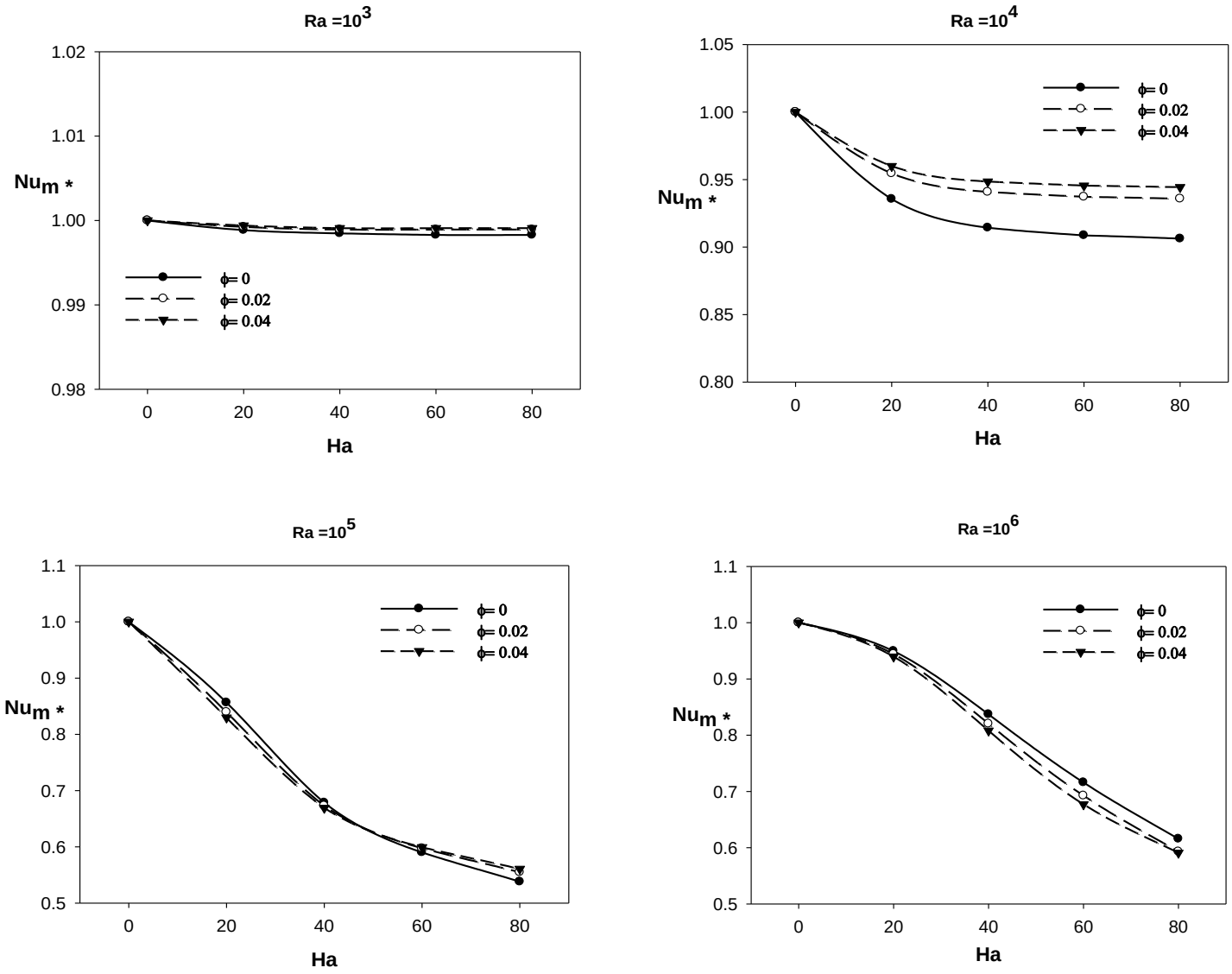

Fig. 10: Effects of Hartmann number on the variation of the average Nusselt number ratio for different nano-particle concentrations.

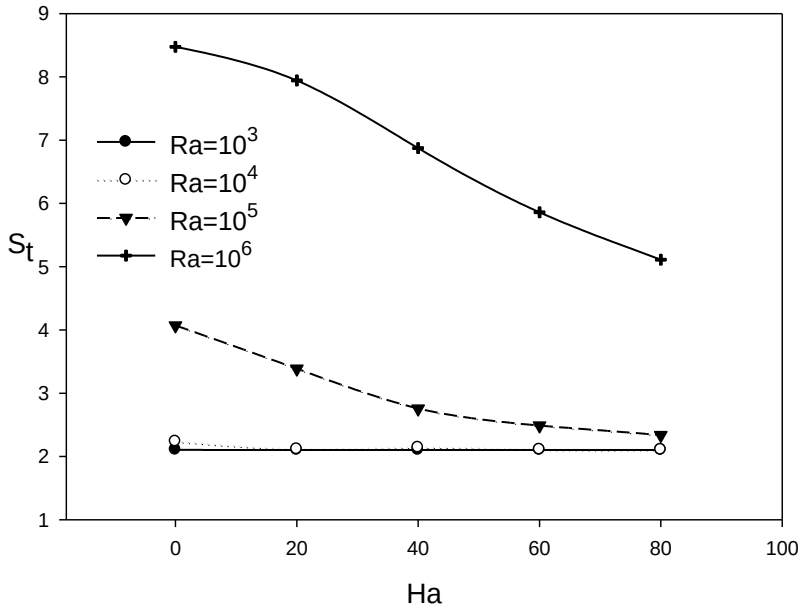

Fig. 11: Effects of Hartmann number on the variation of the Total Entropy at ϕ=0.04.

(a)

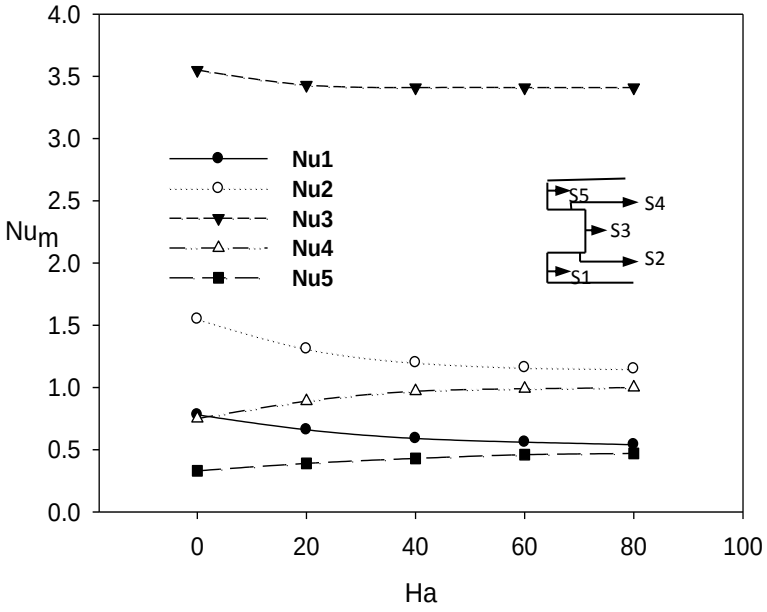

(b)

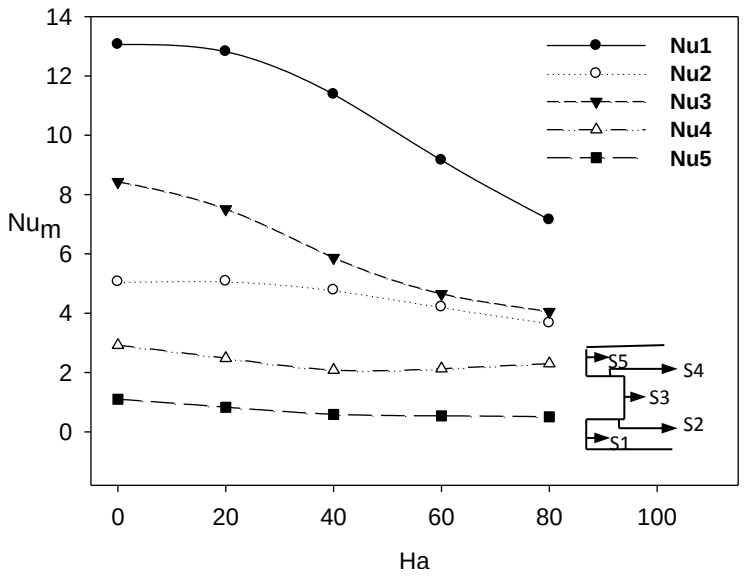

Fig. 12: Effects of Hartmann number on the local Nusselt number at ϕ=0.04 and (a) Ra=10^4 and (b) Ra=10^6.

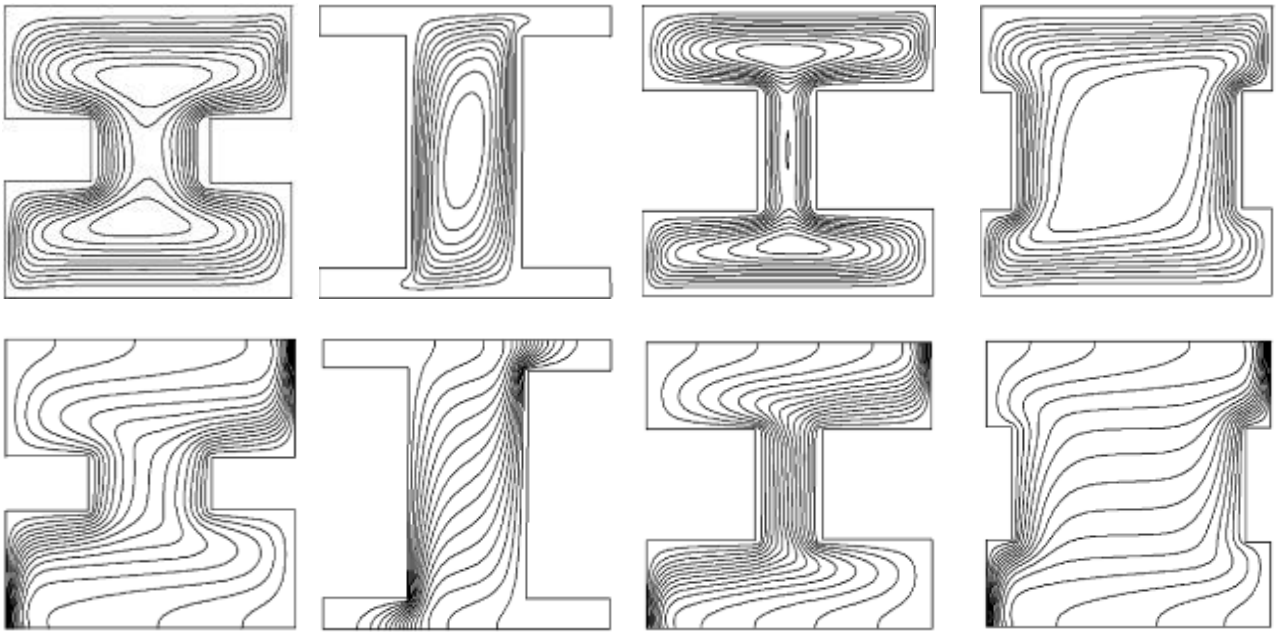

A=0.2 ,B=0.4 *A=0.8 ,B=0.4* *A=0.4 ,B=0.2* *A=0.4 ,B=0.8*

Fig. 13: Streamline (top) and isotherms (bottom). Ra=10^6, ϕ=0.04, Ha=40.

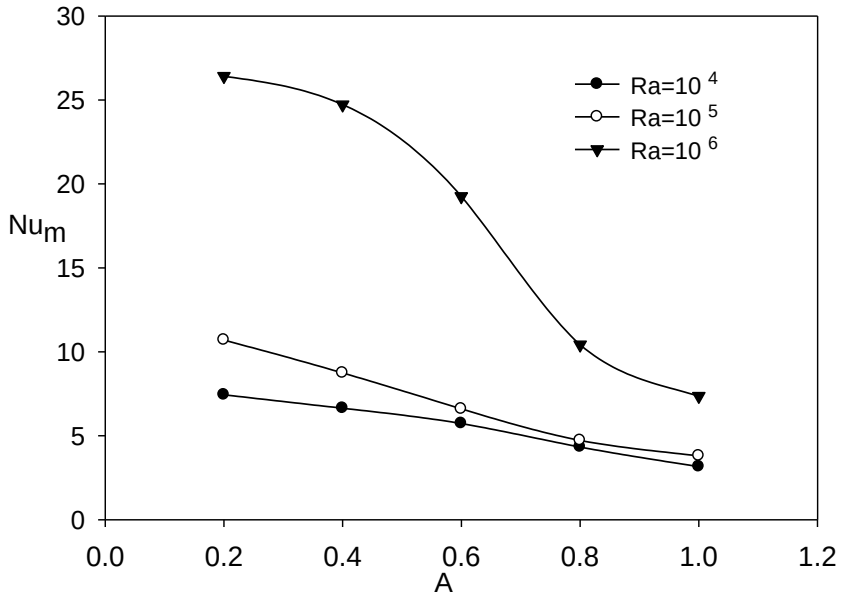

Fig. 14: Effects of variations in the distance of the enclosure flaps, *A*, on the average Nusselt number, ϕ=0.04, Ha=40.

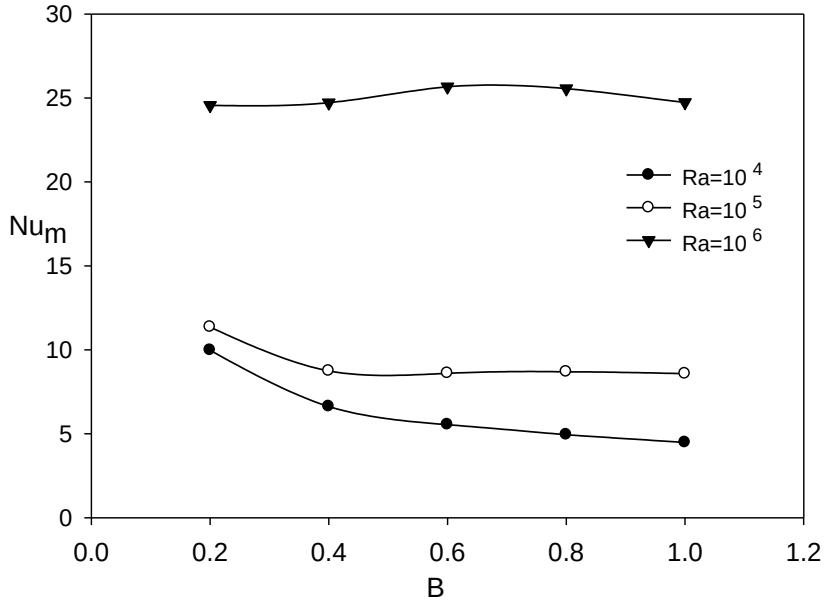

Fig. 15: Effects of the thickness of enclosure connector, *B*, on the average Nusselt number, ϕ=0.04, Ha=40.

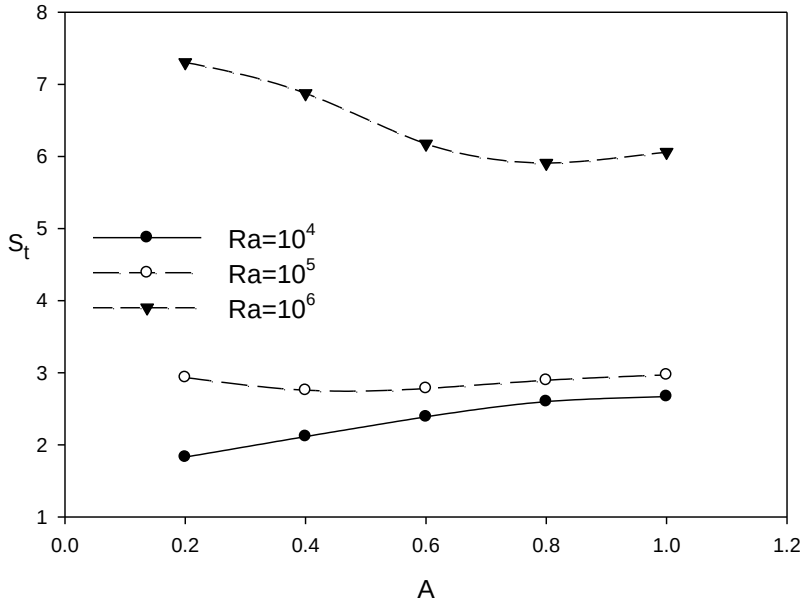

Fig. 16: Effects of variations in the distance of the enclosure flaps, *A*, on the Total Entropy generation, ϕ=0.04, Ha=40, *B*= 0.4.

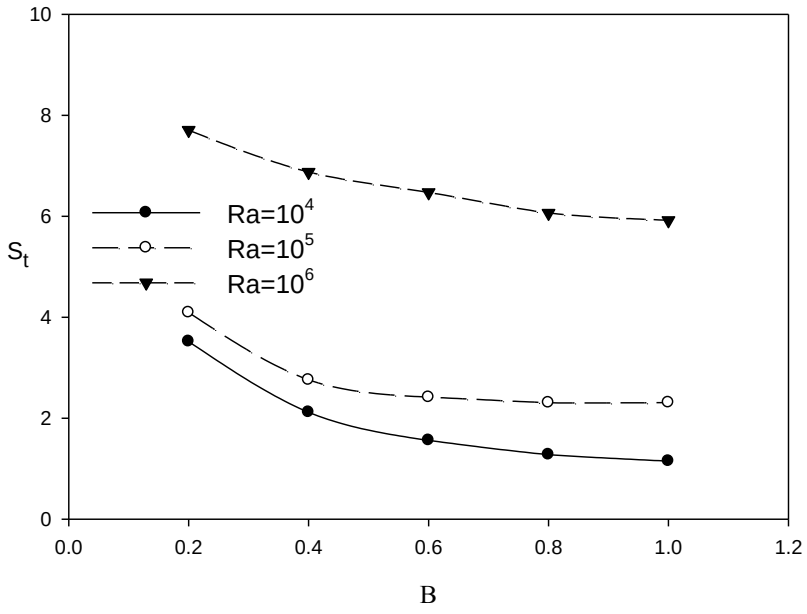

Fig. 17: Effects of the thickness of enclosure connector, *B*, on the total entropy generation, ϕ=0.04, Ha=40, *A*= 0.4.